Validation strategy of reduced-order two-fluid flow models based on a hierarchy of direct numerical simulations

Pierre Cordesse, Angelo Murrone, Thibaut Ménard, Marc Massot

Validation strategy of reduced-order two-fluid flow models based on a hierarchy of direct numerical simulations

Pierre Cordesse[1,2], Angelo Murrone[1], Thibaut Ménard[3] and Marc Massot[2]

[1]ONERA, 8 Chemin de la Hunière, 91120 Palaiseau, France

[2]CMAP, Ecole polytechnique, Route de Saclay 91128 Palaiseau Cedex, France

[3] CNRS UMR 6614 - CORIA, 76801, Saint Etienne du Rouvray cedex, France

pierre.cordesse@polytechnique.edu

Keywords: two-phase flow, reduced-order model, diffuse interface model, direct numerical simulation

Abstract

In industrial applications, the use of reduced-order models to conduct numerical simulations on realistic configurations as a predictive tool strengthen the need of assessing them. In the context of cryogenic atomization, we propose to build a validation strategy of large scale two fluid models with subscale modelling based on a hierarchy of direct numerical simulation test cases to qualitatively and quantitatively assess these models. In the present work, we propose a validation of these reduced-order model relying on DNS on an hierarchy of specific test cases. We propose in this work to investigate an air-assisted water atomization using a planar injector. This test case offers an atomization regime, which makes it worthy to eventually validate our reduced-order models on a cryogenic coaxial injection.

Introduction

Rocket engines safety is one of the main priorities given to space industry. In a cryogenic combustion chamber, the multi-scale and multi-physical phenomena are very complex and their interaction still animate a research domain. In particular, the primary atomization plays a crucial part in the way the engine works, thus must be thoroughly studied to understand its impact on high frequencies instabilities. The latter have been encountered in the past and can lead to critical damages of the rocket. Even though experimentations must be conducted to enable simulation validation and to understand the observed physical phenomena, predictive numerical simulations are mandatory, at least as a complementary tool to understand the physic and even more to conceive new combustion chambers and predict instabilities they may generate in a given configuration.

In sub-critical condition, downside a air-assisted coaxial injector engenders three two-phase flow topologies: at the injector exit, the two phases are separated by a smooth interface. Downstream a polydisperse spray of droplets is carried by the gaseous phase. In between, shear stress caused by strong velocity gradients tears the liquid core apart and ligaments are formed. This process is called primary atomization. The ligaments get thinner and thinner until they break into droplets during the secondary atomization process. In this *mixed region*, the subscale physics and the topology of the flow are very complex. The typical range of flow numbers in sub-critical cryogenic cylindrical jet in real configuration are: for the liquid Reynolds number, $Re_L = 1e^5$, for the hydrodynamic Weber number, $We_H = 1e^5$. On the Mascotte test bench at ONERA, the flows numbers are both an order of magnitude less. As for the ambient pressure, p, it reaches $p = 25\,bar$.

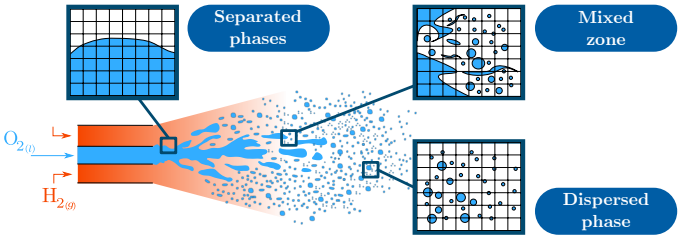

Figure 1: Jet atomization flow topologies

Direct numerical simulations (DNS) in real configuration of such engines are still out of reach, CPU needs being too high due to the high Reynolds and Weber numbers, predictive numerical tools using reduced-order models must be developed. However great care must be taken on the choices of these models in order to both have solid mathematics properties and lead to predictive simulations after a validation process.

The strategy retained to perform a numerical simulation of the primary atomization from the injection to the combustion of the spray is to couple a Kinetic-Based-Moment Methods (KBMM) to describe the disperse flow as in [1] with a diffuse interface model for the separated phases and the mixed zone. Among the hierarchy of diffuse interface model, we focus on the Baer-Nunziato model [2] accounting for full disequilibrium of the phases.

In the present work, we propose a validation of these reduced-order model relying on DNS on an hierarchy of specific test cases. In [3], we have started with an air-assisted water atomization using a coaxial injector, which also provides experimental results from the LEGI test bench. The comparison has shown good agreements in terms of liquid core length and important CPU gains between the *seven equation model* implemented in the CEDRE code [4] and the DNS results from the ARCHER code. It has also shown the limits of diffuse interface models to capture complex liquid structures such as ligaments, rings or deformed droplets and encourages to add a sub-scale description of the interface dynamics through geometric variables such as the interfacial area density, the mean and Gaussian curvatures as proposed in [5].

We propose here a second test case, an air-assisted water atomization using a planar injector, which reproduces in terms of Weber and Reynolds number the liquid sheet flowing out a swirling atomizer used in agricultural applications [6], $Re_L = 1.5e^4$ and $We_R = 4.0e^2$ and $p = 1\,bar$. The DNS results obtained thanks to the code ARCHER [7] denotes that this test case offers an atomization regime, which makes it complementary with the first test case in order to eventually validate our reduced-order models on a cryogenic coaxial injection.

In the first part, we will recall the mathematical properties of the models solved. Then, we explain the numerical methods implemented in the two code, CEDRE and ARCHER. Finally, we present the results obtained by both simulations and compare them.

1 Mathematical modelling

At the top of the hierarchy of diffuse interface models [8, 9] stands the Baer-Nunziato model [2], also called the *seven equation model*, accounting for full disequilibrium of the phases. This first-order non-linear non-conservative system of partial differential equations is composed of a mass, momentum and energy equation for each phase and a seventh equation on the volume fraction α to reconstruct the interface. The extended form proposed in [10] introduces an interfacial pressure, p_I, and an interfacial velocity, v_I, that need to be closed. From this seven-equation model, the instantaneous relaxation of the pressures and the velocities leads to the *five-equation* model [11] and relaxing also instantaneously the temperatures, one obtains the compressible multi-species Navier-Stokes equations referred as the *four-equation* model. These three models define a hierarchy of diffuse interface model and each of them are hyperbolic and appropriate for reactive two-phase flow or interface problems.

In cryogenic applications, the pressure of the phases may be considered to relax instantaneously, but due to the strong velocity and temperature gradients at the interface, it is unrealistic to assume hydrodynamic and thermal instantaneous relaxations. Whereas single velocity models are sufficient in the separated zone with an adapted resolution mesh, it is not the case in the mixed region and thus fail at predicting the atomization process. Therefore the Baer-Nunziato model appears as the best two-velocity model candidate for the present study.

Nonetheless, stemming from rational thermodynamics, the macroscopic set of equations can not be derived from physics at small scale of interface dynamics and thus require closure of interfacial pressure and velocity as well as to postulate the thermodynamics. The theory on the existence of a supplementary conservative equation to first-order order system of partial differential equation including non-conservative terms [12, 13] has brought about supplementary conservative equations together with constraints on the interfacial quantities and the definition of the thermodynamics of the mixture. In this work, we use a non-miscible fluid thermodynamic, where the mixture entropy is defined by the mass averaged sum of the phasic entropies with no mixing effect, together with an closure proposed in [14] obtained through a discrete element method approach [15]. To the convection part described in [14], we let the two phases relax towards an equilibrium state thanks to sources terms. Only mechanical, and hydrodynamic relaxations are accounted for in the present study. They are modelled as in [14] through a pressure difference term and a drag term. Each term is driven by a characteristic time, which can be either finite to account for disequilibrium, or in the limit of a zero characteristic time, to account for an instantaneous relaxation and kill all the disequilibrium.

The direct numerical simulation solves the incompressible Navier-Stokes equations and takes into account surface tension. Then, the interface is implicitly derived by the zero of a level set of a scalar function and its motion is captured by the transport of the level set function at the hydrodynamic speed, combined with a projection technique [16]. To guarantee the conservation of mass, we also transport the volume of fluid function (VOF), defined as the liquid volume fraction expressed in terms of the level set function. The benefits of a VOF formulation coupled with a Level Set function are to conserve mass and to have access to geometrical properties of the interface.

2 Numerical methods

The numerical methods employed to solve the Baer-Nunziato model are implemented in the multiphysics computational fluid dynamics software CEDRE [4] working on general unstructured meshes and organized as a set of solver [4]. The solver *SEQUOIA* is in charge of the diffuse interface model whereas the solver *SPIREE* takes care of the droplets once atomized.

A Strang splitting technique is applied on a multi-slope HLLC with hybrid limiter solver [14, 17] to achieve a time-space second-order accuracy on the discretized equations. The issue encountered when discretizing the non-conservative terms is tackled in [14] by assuming (1) the interfacial quantities p_I and u_I to be local constants in the Riemann problem, (2) the volume fraction to vary only across

the interfacial contact discontinuity u_I. As a result, the non conservative terms vanish, u_I and p_I are determined locally by Discrete Equation Method (DEM) [15] at each time step and stay constant during the update. Thus, phases are decoupled the system splits into two conservative sub-systems to which we apply the multi-slope HLLC with hybrid limiter solver.

Depending on the application, the relaxations are assumed either instantaneous or finite in time. In the present test case, it is reasonable to assume a instantaneous pressure relaxation but one need to consider a finite velocity relaxation since the interface dynamic is mainly driven by the shear stress induced by a high velocity difference between the phases at the injection.

To obtain the relaxed pressure, one needs to solve an simple ODE. Since the characteristic time is taken to be infinitely small, the problem reduces to apply an iterative procedure as a Newton method to solve a second order equation and obtained a single equilibrium pressure. Detailed of the equation can be found in [14]. As for the velocities, since we want to account for finite relaxation time, the associated ODE takes the form:

$$\partial_t v_d - \frac{A^o}{\epsilon_v} v_d = 0, \text{with } A^o = \frac{\alpha_1^o \rho_1^o + \alpha_2^o \rho_2^o}{\alpha_1^o \rho_1^o \alpha_2^o \rho_2^o}, \qquad (1)$$

where v_d is the slip velocity, ϵ_v is the characteristic relaxation time and superscript ^{o} denotes the state before relaxation and α_k, ρ_k denote respectively the volume fraction and the partial density of phase k. A first numerical approach is to fix a remaining slip velocity ratio target at each computational time step Δt. It defines the characteristic relaxing time as

$$\frac{\epsilon_v}{A^o} = \ln\left(\frac{v_d(\Delta t)}{v_d^o}\right)\Delta t. \qquad (2)$$

An instantaneous velocity relaxation is in practice also possible and manipulating the ODE leads to a unique relaxed velocity, which is the mass weighted average of the two velocities before relaxing.

As for the DNS, as mentioned by Rudman [18], it is recommended to solve Navier-Stokes equations in their conservative form to ensure consistance between mass, VOF, and momentum fluxes. Because a staggered grid is adopted, VOF and velocity have not the same control volume making it difficult to stay consistant. To avoid the finest grid for the VOF transport proposed in [18] to preserve consistency, the method developed in [7] is used here and permit to reduce time computation.

The Navier-Stokes equations are implemented in the code ARCHER [7]. A projection method is employed and physical properties (viscosity and density) are expressed in term of both VOF and Level Set. The temporal integration is performed through a second-order Runge-Kutta scheme. The discretization of convective term is achieved with WENO 5 scheme [19]. For the viscosity term, we retain the method presented by Sussman [20]. The Ghost-Fluid [21] method is employed to take into account surface tension, treated as a pressure jump.

To compute correctly mass fluxes at the interface (consequently momentum fluxes) and to preserve consistency between both flow and interface solvers, VOF and Level set transport are performed with a CLSVOF algorithm [22] at each step of Runge Kutta scheme.

3 Description of the configuration

To attest the reduced-order model introduced in Section 1 with direct numerical simulation, we propose an air-assisted flat liquid sheet at high Reynolds and Weber number, inspired from a swirling injector used for agriculture [6]. This test case contributes to the validation strategy based on an hierarchy of direct numerical simulation test cases that eventually wants to reproduce an air-assisted coaxial atomization of liquid in cryogenic rocket engines and started in [3].

Air-assisted flat liquid sheets have been widely experimentally investigated such as in [23]. The behaviour of such flow is mainly driven by four parameters. The ratio V_G/V_L and the momentum flux ratio M determine the breakup regime. Then the width of liquid injection, D_L and the relative gaseous Weber number, We_R, influence the breakup length, the breakup frequency and the liquid sheet vibrating frequency [23]. M and We_R are defined in Equation (3).

$$M = \frac{\rho_G V_G^2}{\rho_L V_L^2}, \qquad We_R = \frac{\rho_G (V_G - V_L)^2 D_L}{\sigma}. \qquad (3)$$

Other classical flow parameters exist such as the liquid Reynolds number, $Re_L = \rho_L V_L D_L/\mu_L$, the gas Reynolds number, $Re_G = \rho_G V_G (D_G - D_L)/\mu_G$, the liquid Weber Number, $We_L = \rho_L V_L^2 D_L/\sigma$, the gas Weber Number, $We_G = \rho_G V_G^2 (D_G - D_L)/\sigma$ or the aerodynamic Weber number, $We_H = \rho_G V_G^2 D_L/\sigma$, but they are preferred in cylindrical jet applications.

The present configuration has been obtained by adjusting the flow parameters in order to optimize the flapping amplitude and to guarantee a wide liquid core. The momentum flux ratio is fixed to $M = 1.88$ and the relative gaseous Weber number to $We_R = 403$. No Break-up regimes in the parameter spaces $Re_L - We$ exists for planar jet, as what exists for coaxial jet [24]. However, high relative velocity, as it is the case here, usually leads to strong sinusoidal oscillations of the liquid flow inducing an high spray angle and short sheet breakup length, called "flag-effect" [23]. The DNS results attests these predictions and clearly shows an atomized spray.

The simulated domain described in Figure 2 shows the boundary conditions of the simulation. ① is the liquid injection plan, ② is the gas injection plan, ③ and ③ are periodic plans, ④ , ⑤ and ⑥ are outflow plans. The liquid injection height, D_L, the gas injection height, D_G, the x-y-z length of the box, L_x, L_y, L_z, are given in Table 1. Figure 3 defines the velocity profile of the gas and the liquid, which are symmetric with respect to the x-axis and y-invariant. The gas velocity profile V_G given in Equation (4) is typical for

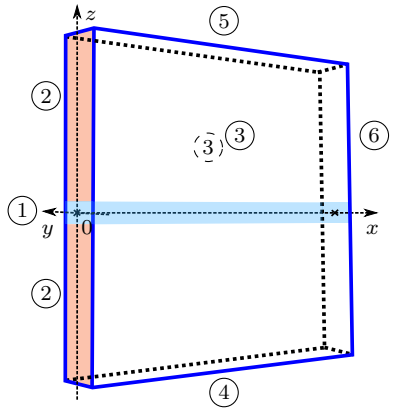

Figure 2: Test case configuration and initial boundary conditions

Table 1: Test case configuration - dimensions

units	D_L	D_G	L_x	L_y	L_z
(mm)	1	16	16	4	16

turbulent pipe flow [25].

$$V_G = V_G^{avg} \frac{7}{6} \left(\frac{2|z| - D_L}{D_G - D_L} \right)^{\frac{1}{6}} + V_L. \tag{4}$$

The average gas velocity V_G^{avg} is $65\,m/s$. An offset equal to $V_L = 1.5\,m/s$ ensures the continuity of the velocity profile at the injection plan. The domain is initially filled with a liquid sheet in the $x-y$ plan, as thick as the liquid slit as shown on Figure 2. Table 2 states the fluid properties in terms of density ρ, surface tension coefficient, σ, and viscosity, μ. The ARCHER simulations are performed on a

Table 2: Physical properties of liquid and gas

Phase	$\rho\ (kg/m^3)$	$p\ (MPa)$	$\sigma\ (N/m)$	$\mu\ (Pa.s)$
Liquid	1000	0.1	0.01	0.0001
Gas	1	0.1	0.01	0.0001

Cartesian mesh $512 \times 128 \times 512$ with a cell size equal to $\Delta x = 3.125\,10^{-5}\,m$, so a total of 101 millions of faces whereas CEDRE mesh is composed of tetrahedral cells with a total of $148k$ faces.

In order to compare the results of the DNS to the results obtained with CEDRE, one must consider the fact that the DNS solver is incompressible, thus there is no acoustic impacting the liquid sheet and its density is constant. To restrain the acoustic role in the CEDRE compressible solver, we have enlarged the computational domain by a factor 5 in the x and z direction and meshed it with a very coarse mesh to avoid any reflecting waves as shown in Figure 4a. The minimum cell size is $\Delta x = 1.0\,10^{-4}\,m$ and can be found along the liquid slit as one notices on Figure 4b.

Furthermore the use of a compressible thermodynamics in CEDRE through the Stiffened-Gas equation of state makes

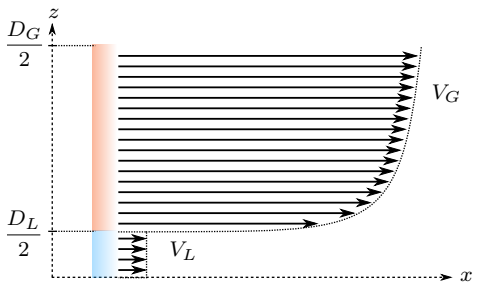

Figure 3: Injector schematic and velocity profiles

it impossible to maintain the liquid density constant. The temperature of the phases have been modified to obtain the same initial pressure and density conditions as in Table 2 and in practice, the liquid density almost stays constant as shown on Figure 5.

The convection time t_{conv} of the system, defined as

$$t_{conv} = \frac{L_x}{V_L}, \tag{5}$$

equals $t_{conv} = 10.7\,ms$. The CEDRE simulation has run $t_{sim} = 27\,ms$. which corresponds to approximately three convective times. The simulation information are summarized in Table (3). The total CPU cost is defined as the prod-

Table 3: Simulation costs comparison for $9\,ms$

	$t_{sim}\ [ms]$	N_{proc}	CPU cost $[h]$
CEDRE	9.0	700	$8.54\,10^3$
ARCHER	9.0	552	$2.83\,10^5$

uct of the number of processors, N_{proc}, times the computational time for a given simulation time, t_{sim}. The CPU difference is notable, ARCHER is 33 more costly than CEDRE.

4 Results and discussion

Before comparing the results from CEDRE to the DNS, we propose to analyze qualitatively and quantitatively the results obtained with CEDRE.

On Figure 6, the instantaneous liquid sheet axial length is plotted with respect to the simulation time t_{sim}. The liquid sheet length is defined with respect to a liquid volume fraction isovalue. Left blue $y-$axis encompasses the whole range of the liquid sheet at the isovalue, $\alpha_l = 0.95$. Initially at a length $L_{lc} = 35\,mm$, the liquid sheet rapidly gets smaller and breaks at $t_{sim} = 2.5\,ms$ to reach an average value of $L_{lc} = 0.8\,mm$ emphasized on the right $y-$axis where two isovalues, $\alpha_l = 0.91$ and $\alpha_l = 0.99$ are used to capture the liquid sheet length. The transient regime lasts around $t = 3\,ms$ during which the initial liquid sheet breaks, the downside part being carried away by the fast flowing air. Then the planar jet starts flapping steadily.

A sensor placed near the injection slit, at $(x, y, z) = (2, 0, 0)\,mm$, has recorded the liquid volume fraction over

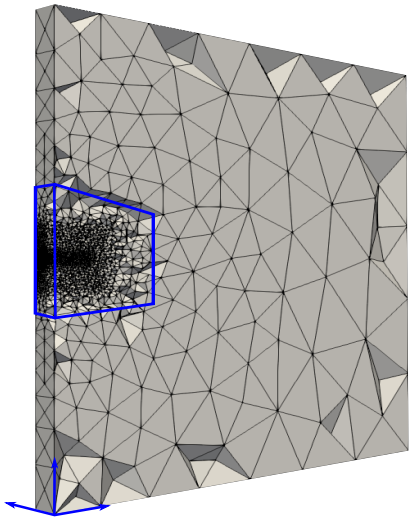

(a) CEDRE mesh

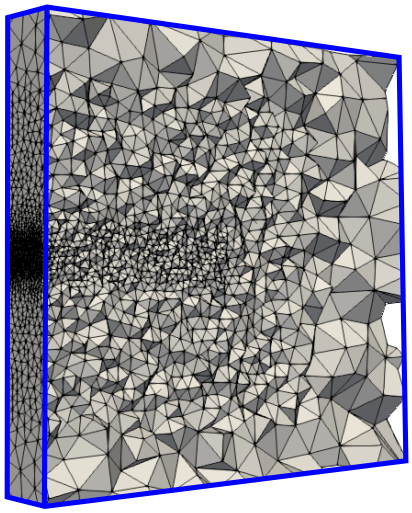

(b) Refined DNS box

Figure 4: CEDRE mesh of the configuration

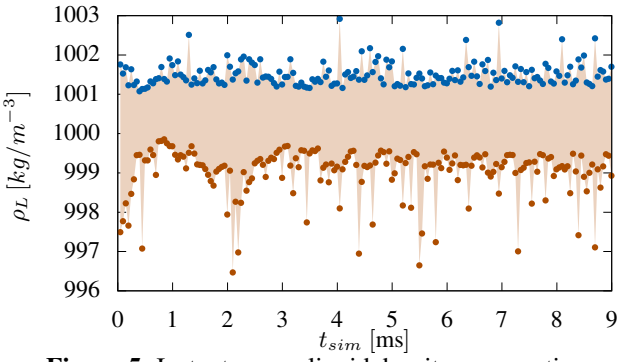

Figure 5: Instantaneous liquid density ρ_L over time, ● maximum value, ● minimum value.

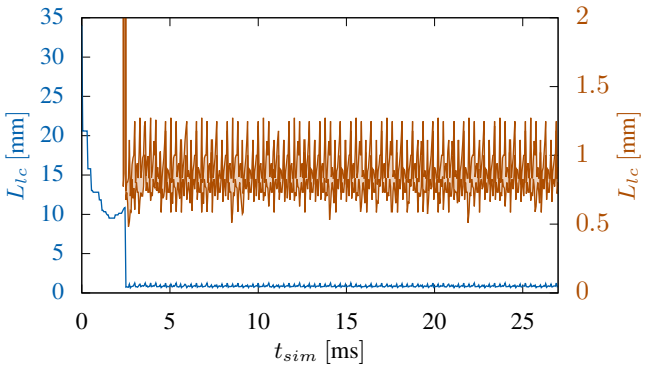

Figure 6: Liquid sheet length L_{lc} over time at isovalue: — $\alpha_2 = 0.95$, — $\alpha_2 \in [0.91, 0.99]$.

time as plotted on Figure 7. The peaks are evenly spaced, but one observes two different height of peaks, suggesting one corresponds to the movement downwards of the sheet and the other corresponds to the movement upwards of the sheet. On Figure 8 is depicted liquid volume fraction contours over time. It emphasizes the sinusoidal flapping to be expected for such flow regime and confirms the two peaks recorded by the probe at $(2, 0, 0)\, mm$. The frequency, f, and the period of the flapping, Δt, are

$$f = 1.7\,10^3\, Hz \qquad \Delta t = 0.59\, ms \tag{6}$$

Many experimental correlations exist for this longitudinal instability, and as observed for example in [26], the frequency is highly depending on velocity profile at the interface at the edge of the slit. It means that this frequency depends mainly on the mesh resolution and it is very unlikely to find the same frequency for different meshes, and thus to compare the results of CEDRE simulation with the DNS.

The two-phase flow model offers a non-instantaneous velocity relaxation of the phases. This disequilibrium is relevant in strong velocity gradient regions such as close to the liquid sheet injection plan. Physically, the liquid is expected to be accelerated by the gas, but not instantaneously. Therefore it is physically wrong to assume an instantaneous relaxation time for the velocities of the phase. The maximum slip velocity norm over time is plotted in Figure 9a with the averaged slip velocity norm in Figure 9b, together with the averaged liquid volume fraction isolines. Interestingly, the slip velocity is not negligible in the flapping zone and is in average $0.3\, m/s$. Numerically, after the velocity relaxing procedure, the remaining slip velocity is only ten percent of the slip velocity before relaxing procedure. It means that in this region, the slip velocity before relaxation is about $3\, m/s$. These results attest the robustness of the solver able to handle velocity slip but also the interest of a two velocity model.

We now propose to compare the liquid sheet obtained with ARCHER and CEDRE at given simulation time. The Level Set function of the DNS permits an exact reconstruction of the interface whereas for the diffuse interface model, the interface lays in the region where the volume fraction varies from $\alpha \approx 0$ to $\alpha \approx 1$. Consequently, in Figure 10 we have superimposed the solved interface of the DNS to a volume rendering of the liquid volume fraction and a single liquid volume fraction isosurface. α_{H_2O} In Figure 10, we distinguish two regions. Close to the injector slit, the diffuse interface model matches the DNS results. The CEDRE mesh used in this region prevents the interface from diffusing too much such that the interface captured by the DNS lays in the volume rendering of the liquid volume fraction of CEDRE.

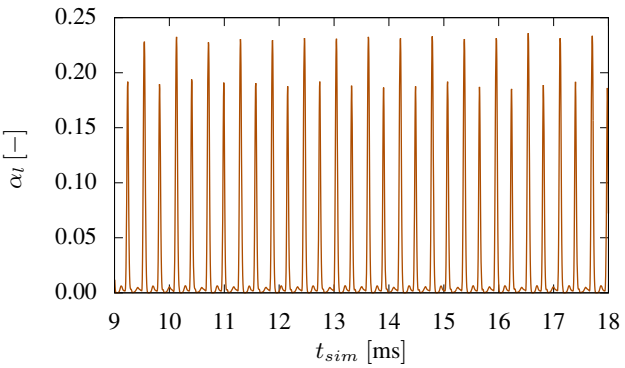

Figure 7: Liquid volume fraction at sensor $(x, y, z) = (2, 0, 0)\, mm$ over time.

The breakup length of the liquid sheet matches qualitatively. Downstream the liquid core of the planar jet in the *mixed region*, the DNS shows complex liquid structures that rapidly become a dense spray. The diffuse interface model is ineffective in capturing these effects and we only see a red cloud corresponding to a low liquid volume fraction isovolume. The reasons of such a discrepancy between CEDRE and the DNS is twofold. First the CEDRE mesh is too coarse compared to the DNS mesh. Second, the volume fraction, alone, is not sufficient to describe such complex interface dynamics. We would need to add a subscale modelling of the interface dynamics as proposed in [5] where a supplementary geometric variable, the interfacial density area, is solved. Finally, this comparison gives an interesting interpretation of the diffuse interface models. The volume fraction is not enough to reconstruct the whole dynamic of the interface but attests to the presence or the absence of liquid.

Conclusions

In the present work, we proposed to pursue the evaluation of reduced-order models to perform predictive simulations of the primary atomization in cryogenic rocket engines. As a baseline comparator, we relied on the DNS results of an hierarchy of specific test cases. We originally started with an air-assisted water atomization using a coaxial injector, in [3], which also provides experimental results from the LEGI test bench. Here we proposed an air-assisted water atomization using a planar injector representative of swirling atomizers found in agricultural applications [6].

The reduced order model was a diffuse interface model offering an non-instantaneous velocity relaxation and was implemented using a Strang splitting technique applied on a multi-slope HLLC solver [14, 17] in the CEDRE code of ONERA [4]. The DNS results were obtained using the incompressible Navier-Stokes equations together with a CLSVOF [22] thanks to the code ARCHER [7]. This test case offers an atomization regime with a dense spray, which makes it complementary with the first test case in order to eventually validate our reduced-order models on a cryogenic coaxial injection.

The comparison has shown good agreements in terms of liquid sheet length near the slit, together with an important CPU

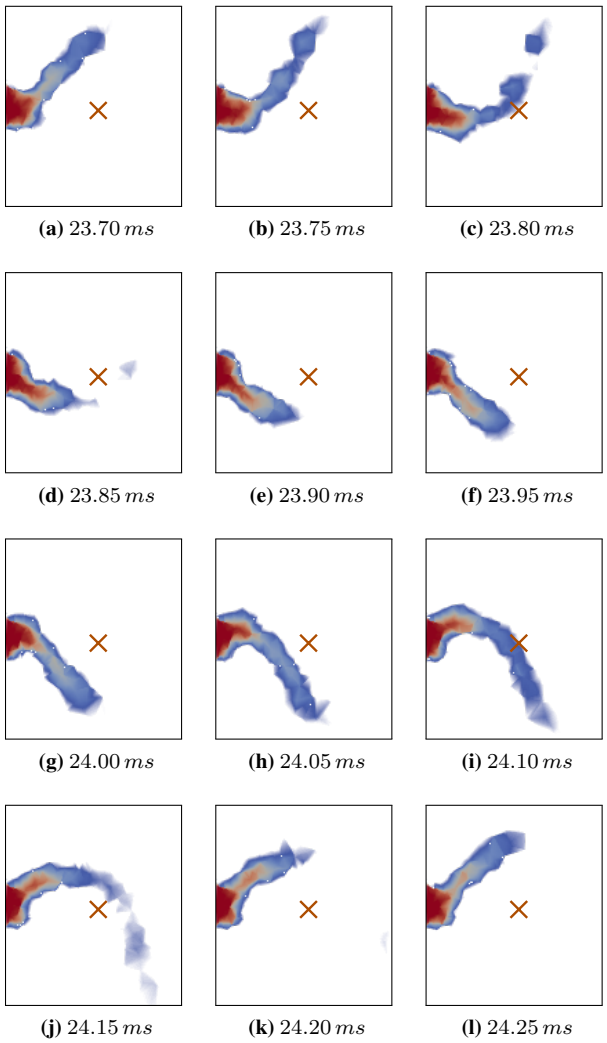

Figure 8: Instantaneous liquid volume fraction near the injector, $\alpha_l = 0.1$ $\alpha_l = 1.0$, probe at $(2, 0, 0)\, mm$ ×

gains between the *seven equation model* implemented in the CEDRE code and the DNS results from the ARCHER code. However, it has shown the limits of diffuse interface models to capture the complex liquid structures departing from the liquid sheet in the *mixed region* due to the coarse CEDRE mesh, but also due to the limitation of the volume fraction to describe the dynamic of the interface. It suggests to add a sub-scale description of the interface dynamics through geometric variables such as the interfacial area density, the mean and Gaussian curvatures as proposed in [5].

In future works, we will first aim at defining a physical dynamic velocity relaxation time. Then, we will add the subscale description of the interface dynamics to obtain a better solution in the mixed region and compare it to the DNS results.

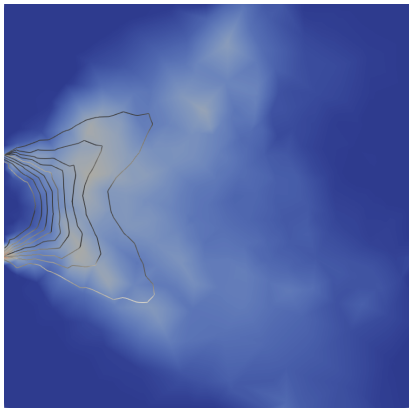

(a) Maximum value over time

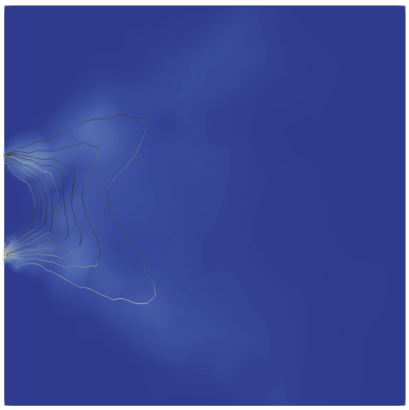

(b) Time average

Figure 9: Contour of slip velocity norm over time, $\|v_d\| = 0\,m/s$ $\|v_d\| = 0.65\,m/s$, and averaged liquid volume fraction isolines, range $[0 : 1]$ by 0.1 increment. Box size is $L_x/4 \times L_z/4$.

Acknowledgments

The support of the French Government Space Agency (CNES) and the French Aerospace Lab (ONERA) through a PhD grant for P.Cordesse, the help of L.H. Dorey (ONERA) and M. Théron (CNES) are gratefully acknowledged. We also thank A. Remigi, CNRS CORIA UMR 6614. Simulations have been successfully conducted using the CEDRE computational fluid dynamic software on the ONERA cluster.

References

[1] Sibra, A., Dupays, J., Murrone, A., Laurent, F., and Massot, M., *Simulation of reactive polydisperse sprays strongly coupled to unsteady flows in solid rocket motors: Efficient strategy using Eulerian Multi-Fluid methods*, J. Comput. Phys. 339:210–246, 2017.

[2] Baer, M. R. and Nunziato, J. W., *A two-phase mixture theory for the Deflagration-to-Detonation Transition (DDT) in reactive granular materials*, Int. J. Multiphase Flow, 12(6):861–889, 1986.

[3] Cordesse, P., Murrone, A., Menard, T., and Massot, M., *Comparative study of jet atomization simulations: direct numerical simulations and diffuse interface models coupled with kinetic-based moment methods*, NASA Technical Memorandum, Summer Program 2018, NASA Ames Research Center, 2018.

[4] Gaillard, P., Le Touze, C., Matuszewski, L., and Murrone, A., *Numerical Simulation of Cryogenic Injection in Rocket Engine Combustion Chambers*, AerospaceLab:16, 2016.

[5] Cordesse, P., Di Battista, R., Kohk, S., and Massot, M., *Derivation of a two-phase flow model with two-scale kinematics and surface tension by means of variational calculus*, NASA Technical Memorandum, Summer Program 2018, NASA Ames Research Center, 2018.

[6] Belhadef, A., Vallet, A., Amielh, M., and Anselmet, F., *Pressure-swirl atomization: Modeling and experimental approaches*, Int. J. Multiphase Flow, 39:13–20, 2012.

[7] Vaudor, G., Ménard, T., Aniszewski, W., Doring, M., and Berlemont, A., *A consistent mass and momentum flux computation method for two phase flows. Application to atomization process*, Computers & Fluids, 152, 2017.

[8] Drui, F., Larat, A., Kokh, S., and Massot, M. "A hierarchy of simple hyperbolic two-fluid models for bubbly flows". in revision for JFM. 2019.

[9] Drui, F., *Eulerian modeling and simulations of separated and disperse two-phase flows : development of a unified modeling approach and associated numerical methods for highly parallel computations*, PhD Thesis, 2017.

[10] Saurel, R. and Abgrall, R., *A Multiphase Godunov Method for Compressible Multifluid and Multiphase Flows*, J. Comput. Phys. 150(2):435–467, 1999.

[11] Kapila, A. K., Menikoff, R., Bdzil, J. B., Son, S. F., and Stewart, D. S., *Two-phase modeling of deflagration-to-detonation transition in granular materials: Reduced equations*, Phys. Fluids, 13(10):3002–3024, 2001.

[12] Cordesse, P., Massot, M., and Murrone, A., *Mathematical modelling of multi-phase flow using entropy symmetrization*, Proceeding, ECCM-ECFD, Glasgow, UK, 2018.

[13] Cordesse, P. and Massot, M., *Supplementary conservative law for non-linear systems of PDEs with non-conservative terms: application to the modelling and analysis of complex fluid flows using computer algebra*, in revision Commun. Math. Phys. 2019.

[14] Furfaro, D. and Saurel, R., *A simple HLLC-type Riemann solver for compressible non-equilibrium two-phase flows*, Computers & Fluids, 111:159–178, 2015.

[15] Saurel, R., Gavrilyuk, S., and Renaud, F., *A multiphase model with internal degrees of freedom : application to shock-bubble interaction*, J. Fluid Mech. 495:283–321, 2003.

[16] Sussman, M., Smereka, P., and Osher, S., *A Level Set Approach for Computing Solutions to Incompress-*

Figure 10: Instantaneous liquid core comparison. CEDRE: volume rendering of the liquid volume fraction, α_{H_2O} high low, grey isosurface $\alpha_{H_2O} = 0.99$. ARCHER: Grey isovolume of liquid volume fraction $\alpha_{H_2O} = 1$

ible Two-Phase Flow, J. Comp. Phys. 114(1):146–159, 1994.

[17] Le Touze, C., Murrone, A., and Guillard, H., *Multislope MUSCL method for general unstructured meshes*, J. Comput. Phys. 284:389–418, 2014.

[18] Rudman, M., *A volume-tracking method for incompressible multifluid flows with large density variations*, Int. J. Numer. Methods Fluids, 28(2):357–378, 1998.

[19] Jiang, G.-S. and Shu, C.-W., *Efficient Implementation of Weighted {ENO} Schemes*, J. Comput. Phys. 126(1):202–228, 1996.

[20] Sussman, M., Smith, K., Hussaini, M., Ohta, M., and Zhi-Wei, R., *A sharp interface method for incompressible two-phase flows*, J. Comp. Phys. 221(2):469–505, 2007.

[21] Fedkiw, R. P., Aslam, T., Merriman, B., and Osher, S., *A Non-oscillatory Eulerian Approach to Interfaces in Multimaterial Flows (the Ghost Fluid Method)*, J. Comput. Phys. 152(2):457–492, 1999.

[22] Sussman, M. and Puckett, E. G., *A Coupled Level Set and Volume-of-Fluid Method for Computing 3D and Axisymmetric Incompressible Two-Phase Flows*, J. Comp. Phys. 162(2):301–337, 2000.

[23] Dumouchel, C., *On the experimental investigation on primary atomization of liquid streams*, Experiments in Fluids, 45:371–422, 2008.

[24] Lasheras, J. C. and Hopfinger, E. J., *Liquid Jet Instability and Atomization in a Coaxial Gas Stream*, Annu. Rev. Fluid Mech. 32(1):275–308, 2000.

[25] Schlichting, H., Boundary - Layer Theory, McGraw-Hill, 1979.

[26] Lozano, A., Barreras, F., Hauke, G., and Dopazo, C., *Longitudinal instabilities in an air-blasted liquid sheet*, J. Fluid Mech. 437:143–173, 2001.